ACS APPLIED ENERGY MATERIALS

www.acsaem.org Article

Metal Cation Pre-Intercalated $Ti_3C_2T_x$ MXene as Ultra-High Areal Capacitance Electrodes for Aqueous Supercapacitors

Kaitlyn Prenger, Yangunli Sun, Karthik Ganeshan, Ameer Al-Temimy, Kun Liang, Chaochao Dun, Jeffrey J. Urban, Jie Xiao, Tristan Petit, Adri C. T. van Duin, De-en Jiang, and Michael Naguib*

Cite This: *ACS Appl. Energy Mater.* 2022, 5, 9373−9382 Read Online

ACCESS | Metrics & More | Article Recommendations | Supporting Information

ABSTRACT: Two-dimensional transition-metal carbides and nitrides "MXenes" have demonstrated great potential as electrode materials for electrochemical energy storage systems. This is especially true for delaminated $Ti_3C_2T_x$, which already shows outstanding gravimetric and volumetric capacitance, with areal capacitance limited by thickness (only a few microns). However, the performance of multilayer $Ti_3C_2T_x$ has been more modest. Here, we report on using metal cation (*viz.*, Na^+, K^+, and Mg^{2+}) pre-intercalated multilayer $Ti_3C_2T_x$ as electrodes for aqueous supercapacitors. These electrodes are scalable and amenable to roll-to-roll manufacturing, with adjustable areal loadings of 5.2 to 20.1 mg/cm^2. K−$Ti_3C_2T_x$ exhibited the highest capacitances at different scan rates. A gravimetric capacitance comparable to that of delaminated MXene of up to 300 F/g was achieved for multilayer K−$Ti_3C_2T_x$ but with an outstanding ultra-high areal capacitance of up to 5.7 F/cm^2, which is 10-fold higher than the 0.5 F/cm^2 of delaminated MXene and exceeds the 4.0 F/cm^2 of microengineered MXene electrodes.

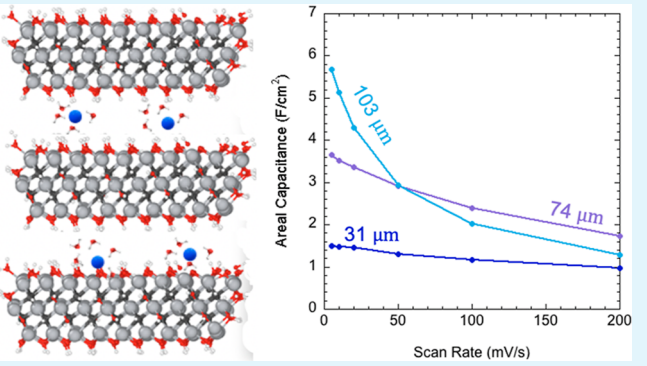

KEYWORDS: *MXene, titanium carbide, intercalation, supercapacitor, areal capacitance*

INTRODUCTION

Electrochemical energy storage is an important frontier as the use of renewable energy sources increases. Modern energy grids will require both batteries and supercapacitors to incorporate renewable energy sources.[1] While batteries display excellent energy density, they have lower power density and thus charging and discharging cycles can take a long time due to the kinetics of the reactions responsible for their charge storage.[1−3] The mechanism for supercapacitors, on the other hand, can be a combination of processes, including surface faradaic processes (pseudocapacitors) as well as electric double layer capacitance (EDLC).[1,2] Because these processes are largely dependent on surface interactions rather than bulk ion transport as in batteries, they have excellent power density, with modest energy density, and are useful for applications where fast cycling is key.[2,3] Pseudocapacitors are able to store energy through fast and reversible redox reactions on material surfaces. Many of the prime candidates for these redox reactions suffer from poor electrical conductivity (*e.g.*, MnO_2 has an electric conductivity of 10^{-5} to 10^{-6} S/cm).[4] Another example for one of the most promising pseudocapacitive materials, RuO_2, is expensive due to the scarcity of ruthenium in the Earth's crust.[1,3,5,6] Therefore, it is necessary to develop high-performance electrode materials with high electrical conductivity and low cost.

MXenes are a large family of electrically conductive two-dimensional (2D) transition-metal carbides and nitrides, first described in 2011.[7−9] MXenes have a core composition of $M_{n+1}X_n$, where M is one or more early transition metals, X is carbon and/or nitrogen, n = 1−4, and they are further terminated by species, denoted T_x, such as −OH, −O, and −F.[7,10−12] MXenes are synthesized by the selective etching of atomically thin metal layers from layered ceramic called MAX phases.[7−9] The etching results in exfoliated multilayer MXene with a mixture of hydrogen bonding and van der Waals forces.[10] As layered materials with weak interlayer bonding, multilayer MXenes are also able to host a number of ions from monovalent and multivalent cations[5,11,13−17] to small molecules[18,19] and even large alkylammonium cations.[20,21] The ability to intercalate ions makes MXenes attractive candidates for many applications such as catalysis,[22] sensing,[23,24] water purification,[25] and electrochemical energy storage.[8,21,26−29] Intercalation of substances such as tetrabutylammonium

Received: March 2, 2022
Accepted: July 4, 2022
Published: July 20, 2022

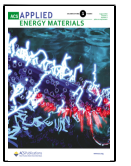

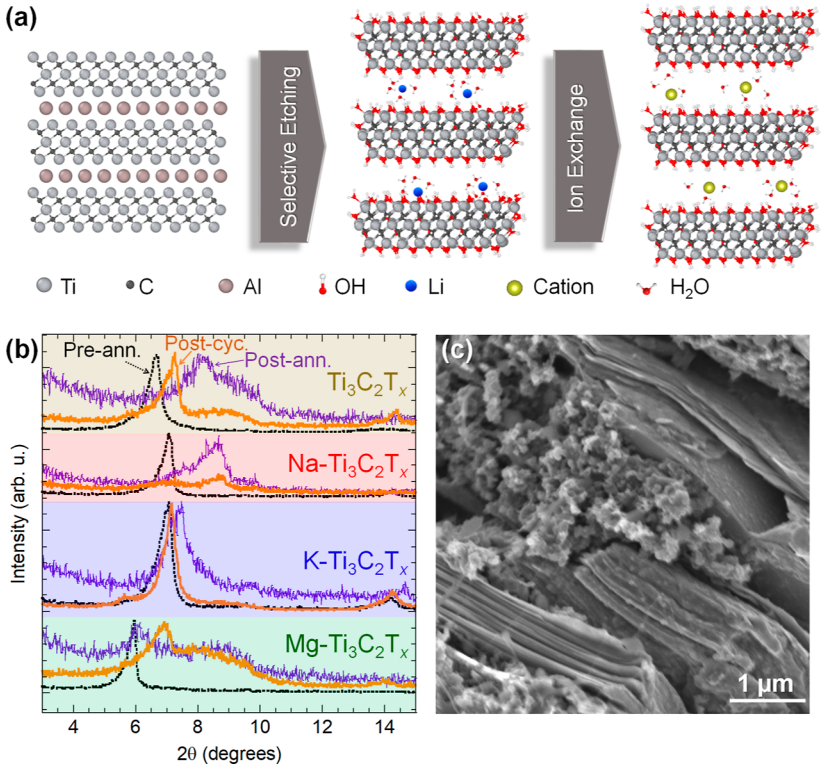

Figure 1. (a) Schematic for intercalation of multilayer $Ti_3C_2T_x$ (OH is used to represent surface terminations for simplicity) by etching using 10 wt % HF with LiCl followed by ion exchange through soaking in ion chloride aqueous solutions. (b) XRD patterns of pristine and intercalated MXene before and after vacuum annealing at 110 °C for 4 h and electrodes after 3000 cycles at 20 mV/s (black lines—before annealing, purple lines—after annealing, and orange lines—after 3000 cycles). (c) Typical cross-sectional SEM image of the prepared electrode, showing multilayer MXene particles (large smooth particles), carbon black (fine particles in clusters), and PTFE threads (faint threads). (This image shows K−$Ti_3C_2T_x$.)

cations[30] and dimethyl sulfoxide[27] can be used to expand the interlayer spacing (*d*-spacing) of MXene, further weakening the intermolecular forces holding the layers together, thus allowing MXenes to be delaminated into single sheets.

When tested as electrode materials for supercapacitors in a sulfuric acid (H_2SO_4) aqueous electrolyte, multilayer MXenes exhibit moderate gravimetric capacitance of around 100 F/g.[6,11,31] On the other hand, electrodes made of delaminated MXene sheets show excellent gravimetric (~400 F/g) and volumetric (>900 F/cm^3) capacitances, but their areal capacitance is limited to about 0.5 F/cm^2 due to their thinness (2−20 μm).[6,11] Various processing can be done to further enhance the areal capacitance of electrodes made of delaminated MXene, such as using it in hydrogel form or making it macroporous[6] and growing other structures onto it such as metal−organic frameworks,[32] but these modifications are labor-intensive and challenging for the roll-to-roll manufacturing process common for commercial supercapacitor production.[6] Similarly, post etching processing with H_2SO_4 coupled with flake-size control has been shown to increase the rate capability at scan rates over 100 mV/s as well as improving areal capacitance to more than 3 F/cm^2, but it suffers from similar commercialization limitations.[33] Since the materials which are both flexible and demonstrate high areal capacitance are important for use in flexible electronics,[34] a scalable method to enhance the areal capacitance of multilayer $Ti_3C_2T_x$ is desirable. This includes producing electrodes more similar to commercially manufactured carbon-based supercapacitor electrodes (~100−200 μm thick, ~10 mg/cm^2).[35]

Intercalation has been used to enhance the capacitance of other MXenes. For example, lithium and sodium intercalated V_2CT_x-delaminated papers were tested in a variety of electrolytes.[36] Na−V_2CT_x showed a gravimetric capacitance over 275 F/g, which is more than double the capacitance of pristine V_2CT_x, and volumetric capacitance over 1300 F/cm^3, which is among the highest volumetric capacitances reported for MXenes.[36] Potassium intercalated few-layer $Ti_3C_2T_x$ was recently demonstrated to enhance performance in potassium-ion hybrid capacitors due to the increased porosity and interlayer spacing as well as optimized solid electrolyte interphase formation.[37] Another study using electrochemical methods to intercalate alkali metal cations into Nb_2CT_x showed that intercalation of lithium led to improved supercapacitor performance in this system.[38] Urea treatment for $Ti_3C_2T_x$ multilayer MXene also increased the volumetric capacitance by 56% and caused more pronounced peaks in the cyclic voltammetry (CV), suggesting more pseudocapacitive behavior as compared to pristine multilayer $Ti_3C_2T_x$.[39] In the same study, X-ray absorption spectroscopy (XAS) showed that the oxidation state of Ti in urea-treated $Ti_3C_2T_x$ was shifted higher than that of the non-intercalated MXene.[39] Molten salt etching yielding $Ti_3C_2T_x$ with Cu/Co between the layers was also used to prepare aqueous supercapacitors with 290 mF/cm^2 areal capacitance.[40] Recently, intercalation of polymers was shown to greatly increase the capacitance of multilayer $Ti_3C_2T_x$ in room temperature (RT) ionic liquid electrolytes, allowing these larger cations into the interlayer spaces during cycling.[21]

https://doi.org/10.1021/acsaem.2c00653
ACS Appl. Energy Mater. 2022, 5, 9373−9382

Ab initio molecular dynamics (MD) of cation-intercalated $Ti_3C_2T_x$ shows that different cations will demonstrate different position and hydration levels when intercalated.[41] Of the cations we studied, K^+ and Na^+ tend to be found very close to the surface of the MXene layers, whereas Mg^{2+} is more centrally located.[41] Our previous study using XAS on cation pre-intercalated $Ti_3C_2T_x$ showed that cation intercalation shifted the Ti L-edge onset for intercalated $Ti_3C_2T_x$ relative to that of pristine $Ti_3C_2T_x$, in all cases shifting the oxidation state higher when compared to non-intercalated $Ti_3C_2T_x$.[5] Also, the change of the Ti L-edge was found to be dependent on the intercalated cation. When the intercalated materials were dispersed in 10 mM H_2SO_4, the titanium oxidation state was much lower, and the differences between different intercalated and non-intercalated $Ti_3C_2T_x$ became negligible.[5]

Herein, we show that pre-intercalation of $Ti_3C_2T_x$ with cations during the synthesis process (Figure 1a) can significantly enhance the electrochemical performance in supercapacitors with H_2SO_4 aqueous electrolytes. This simple modification produces supercapacitors with gravimetric capacitance up to 300 F/g, comparable to those for electrodes made from delaminated layer MXene sheets, but with significant areal capacitance of up to 5.7 F/cm^2, without excessive nano-engineering of the electrodes. We used XAS to demonstrate the effect of these intercalants on the oxidation state of Ti, which was supported with DFT calculations. Finally, ReaxFF calculations were used to understand the dynamics of the intercalated cations.

EXPERIMENTAL SECTION

Synthesis of Intercalated $Ti_3C_2T_x$. Ti_3AlC_2 was synthesized similarly to previously published reports.[5,42] Briefly, titanium (Ti, 99.5%, -325 mesh, Alfa Aesar), aluminum (Al,99.5%, -325 mesh, Alfa Aesar), and graphite (C, 99%, APS 7−11 μm, Alfa Aesar) powders were mixed in an atomic ratio of 3.00:1.20:1.88, respectively, using yttrium-stabilized zirconia balls in a Turbula T2F mixer for 3 h. The powders were then heated in a tube furnace under flowing argon, Ar, at a heating rate of 10 °C/min until it reached 1600 °C, held at that temperature for 2 h, and then was allowed to cool down in the furnace to RT. Cation-intercalated $Ti_3C_2T_x$ samples were produced similarly to previous work.[5,14,15] Ti_3AlC_2 was ground and sieved to a -325 mesh and then slowly added to a solution of lithium chloride (LiCl, 98.5%, Fisher) in 10 wt % aqueous hydrofluoric acid (HF, 48−51%, Sigma-Aldrich) with a ratio of 1 g of Ti_3AlC_2 to 10 mL of etching solution, in which the molar ratio of Ti_3AlC_2/LiCl was 1:5. The reaction mixture was stirred for 24 h at RT. After etching, the powders were washed with excess deionized (DI) water until a pH > 6 was reached. The wet powders were washed with 37% hydrochloric acid (HCl, Fisher), with a ratio of 30 mL of HCl solution to 1 g of powder. This was centrifuged, and the supernatant was discarded. Another 30 mL of HCl solution for each 1 g of powder was added again to the centrifuging vial, and the sedimented powders were redispersed using vortex. This acid washing step was performed 5 times in total. After the acid washing steps, the powders were washed with excess DI water until a pH > 6 was reached again. The washed wet powders were divided into four equal portions, and each portion was soaked in 40 mL of a solution of 1 M NaCl, 1 M KCl, 0.5 M $MgCl_2$, or 1 M HCl (for non-intercalated MXene, hereafter labeled pristine MXene) at RT for 1 h and then centrifuged, discarding the supernatant. The powders were again soaked in fresh solutions (same as the ones in the latest step) at RT for 24 h. Finally, the mixtures were washed with DI water 3 times, discarding supernatants at each step. The intercalated powders of Na−, K−, and Mg−$Ti_3C_2T_x$ MXenes, and pristine $Ti_3C_2T_x$ were dried by vacuum-assisted filtration.

Characterization. X-ray diffraction (XRD) patterns for all $Ti_3C_2T_x$ samples were obtained using a Rigaku DMAX 2200 Cu Kα X-ray diffractometer using a step size of 0.02° and a 1°/min dwell time. Silicon was used as an internal reference in powder samples. Some samples for XRD were also vacuum-annealed for 4 h at 110 °C to remove bulk water. Scanning electron microscopy (SEM) images were taken using a Hitachi 4800 field effect scanning electron microscope with an accelerating voltage of 3 KeV. To confirm full etching and cation intercalation, energy-dispersive X-ray spectroscopy (EDS) was performed with an accelerating voltage of 30 KeV using a Hitachi 3400 scanning electron microscope with an Oxford EDS tube and Inca software. EDS was performed on as-synthesized powders and electrodes after galvanostatic testing.

Preparation of Supercapacitor Electrodes and Electrochemical Cells. Electrodes were prepared by mixing 90 wt % $Ti_3C_2T_x$ with 5 wt % carbon black (Fisher) and 5 wt % polytetrafluoroethylene (PTFE) (60 wt % dispersion in H_2O, Alfa Aesar) in ethanol as a solvent. The slurry was mixed with a mortar and pestle and then hand-rolled to produce a flexible freestanding electrode with controlled thickness in the ranges of 30−35 μm (areal loading of 4.2−5.2 mg/cm^2), 70−77 μm (areal loading of 10.2−13.4 mg/cm^2), and 100−105 μm (areal loading of 20.1 mg/cm^2). A cross-sectional SEM image of a typical electrode (in this case, K−$Ti_3C_2T_x$) is shown in Figure 1c, where the multilayer MXene and carbon black can be seen in a network of PTFE fibers. Counter electrodes of 95 wt % YP50 Kuraray active carbon (MTI Corp.) and 5 wt % PTFE with ethanol as the solvent were prepared in the same manner. The electrodes were dried by annealing at 110 °C for 4 h in a vacuum oven. These electrodes were cut using a 5 mm diameter punch and assembled into Swagelok three-electrode cells with an aqueous 1 M H_2SO_4 electrolyte using glass fiber separator and glassy carbon current collectors. Active carbon counter electrodes with a weight of more than 3 times the working electrode weight were used. The reference electrode used was Hg/Hg_2SO_4 with a 1 M H_2SO_4 supporting electrolyte. All voltages reported here are *versus* Hg/Hg_2SO_4. It is worth noting that when the commonly used Ag/AgCl reference electrode in the 1 M KCl supporting electrolyte was used in the H_2SO_4 electrolyte, potassium leaching from the supporting electrolyte took place and potassium was detected in the MXene electrodes. To eliminate the possible effect of external potassium on the performance of the MXene electrode, Hg/Hg_2SO_4 with the 1 M H_2SO_4 supporting electrolyte was used here. All the voltages reported here are vs Hg/Hg_2SO_4.

Cells were tested using a Bio-Logic VMP3 potentiostat to collect electrochemical impedance spectroscopy (EIS), CV, and galvanostatic cycling with potential limitation (GCPL). EIS with a frequency range from 300 kHz to 10 mHz with a sinus amplitude of 10 mV was measured after 1000 precycles of CV at 100 mV/s. CV curves were collected, after precycling and EIS, in a voltage window from −0.2 to −1.2 V and scan rates of 5, 10, 20, 50, 100, and 200 mV/s. GCPL testing was conducted between −0.2 and −1.2 V at a specific current of 5 A/g.

X-ray Absorption Spectroscopy. XAS measurements were performed at the U49/2 PGM-1 beamline of the synchrotron BESSY II using the LiXEdrom endstation. The spectra were recorded in total electron yield mode after sticking the dry MXene electrode onto a conductive tape. For the MXene sample dispersed in 1 M H_2SO_4, a drop of the solution was cast on a conductive silicon substrate for measurements.

X-ray Photoemission Spectroscopy. The X-ray photoelectron spectroscopy (XPS) measurements were performed on the as-prepared powder samples using the K-Alpha XPS System from Thermo Scientific. The photon source was a monochromatized Al K_α line ($h\nu$ = 1486.6 eV). The spectra were acquired using a spot size of 400 μm and constant pass energy. A combined low energy electron/ion flood source was used for charge neutralization. A vacuum transfer vessel was used to protect the sample from oxidation. Data were processed using CasaXPS software, and the high-resolution regions were fitted after correcting using adventitious carbon in the C 1s scan.

Computational Details. DFT calculations were performed by using the Vienna ab initio Simulation Package.[43] The projector-augmented wave potential was used to treat the nuclei−electron

https://doi.org/10.1021/acsaem.2c00653
ACS Appl. Energy Mater. 2022, 5, 9373−9382

Table 1. Peak Positions of the (002) Peaks in Intercalated $Ti_3C_2T_x$ for Powder Samples before and after Annealing and for Electrodes after 3000 Cycles

	pre-annealing		post-annealing		post-cycling	
	2θ (°)	d (Å)	2θ (°)	d (Å)	2θ (°)	d (Å)
pristine $Ti_3C_2T_x$	6.67	13.25	8.29[a] & 9.02[a]	10.67 & 9.79	7.29 & 9.06[a]	12.11 & 9.75
Na−$Ti_3C_2T_x$	7.14	12.37	7.20[a] & 8.35[a]	12.26 & 10.58	6.99 & 8.43[a]	12.63 & 10.48
K−$Ti_3C_2T_x$	7.08	12.47	7.31	12.06	5.78[a] & 7.16	15.28 & 12.34
Mg−$Ti_3C_2T_x$	5.97	14.79	6.11[a] & 8.86[a]	14.47 & 9.98	6.90[a] & 8.1[a]	12.80 & 10.9

[a]Signficantly broad peak.

interaction.[44] The Perdew−Burke−Ernzerhof functional within the generalized gradient approximation was used for the electron exchange−correlation.[45] An energy cutoff of 500 eV was chosen for the plane wave basis sets. The DFT-D3 method was adopted to include the van der Waals interaction.[46] All degrees of freedom were relaxed with convergence criteria of 10^{-5} eV in energy and 0.01 eV/Å in force.

A 1 × 1 × 2 supercell containing two AB-stacked $Ti_3C_2O_2$ formula units was adopted to model Na/K pre-intercalated MXene, while a 1 × 2 × 2 supercell containing four AB-stacked $Ti_3C_2O_2$ units was used for Mg pre-intercalated MXene. *k*-point meshes of 7 × 7 × 1 for Na/K−$Ti_3C_2T_x$ and 7 × 4 × 2 for Mg−$Ti_3C_2T_x$ were employed to sample the Brillouin zone. The oxidation states were estimated by the correlation between the nominal oxidate states and the Bader charges.[47−49]

The ReaxFF reactive force [A,B] field-based MD simulations were performed using the AMS suite distributed by SCM (see www.scm.com), with the updated parameters for the $Ti_3C_2T_x$ MXene force field from our recent work.[50] A 24.90 × 27.70 Å layer of $Ti_3C_2T_x$ [T_x: 50% O_2, 50% $(OH)_2$] was first solvated in bulk water at 600 K *NVT*-MD simulation until the edges were terminated with OH-groups from water dissociation. This was followed by the intercalation of K^+ using grand canonical Monte Carlo (GCMC) to ensure energetically optimal placement of K^+ over the MXene surface. The GCMC simulation was terminated once ∼0.11 K^+ per 3 Ti were intercalated. The K^+ intercalated, edge-terminated $Ti_3C_2T_x$ MXene layer was then placed in a 54.57 × 55.64 × 13.18 A periodic cell solvated by a 4 M H_2SO_4 solution. This system, comprising 3586 atoms, was first equilibrated under *NPT*-MD simulation at 300 K and 1 atm for 200 ps, followed by an *NVT*-MD simulation at 500 K for 1.48 ns for data gathering. The elevated temperature and higher concentration of H_2SO_4 were chosen to accelerate the dynamics within the sampling time and length scales of the simulations.

RESULTS AND DISCUSSION

Pre-intercalated MXenes used here were synthesized by selective etching of Al from Ti_3AlC_2 using lithium chloride dissolved in HF followed by ion exchange to replace Li^+ by other cations (*viz.*, Na, K, and Mg) as shown in Figure 1a. EDS of the as-synthesized MXenes, after normalizing these values to 3Ti, showed that pre-intercalated MXenes have values of 0.13 Na, 0.11 K, and 0.06 Mg per $Ti_3C_2T_x$ formula unit for Na−$Ti_3C_2T_x$, K−$Ti_3C_2T_x$, and Mg−$Ti_3C_2T_x$, respectively (Table S1). Based on the EDS (Table S1) and XRD (Figure 1b) analyses, the cation intercalation procedure was successful.

Since the electrodes we used in this study were vacuum-annealed before using, it is important to study the material in both hydrated and annealed states. XRD patterns at around the (002) peak (Figure 1b, Table 1) before and after vacuum annealing at 110 °C for 4 h confirm that ions remain even after water is deintercalated from in-between the MXene sheets. Prior to annealing, the positions of the (002) peaks for pre-intercalated MXenes at 2θ of around 7° are shifted relative to the peak for pristine $Ti_3C_2T_x$ MXene, and some differences remain even after annealing. The position of the (002) peak of Mg−$Ti_3C_2T_x$ shows the greatest deviation from the position of the pristine MXene, shifting from 6.67° 2θ (*d*-spacing = 13.25 Å) in pristine $Ti_3C_2T_x$ to a much lower 2θ of 5.97° that corresponds to a *d*-spacing of 14.79Å. This agrees well with previous studies of Mg−$Ti_3C_2T_x$, as Mg^{2+} intercalates with a hydration shell around it.[15,41] After annealing, Mg−$Ti_3C_2T_x$ has a very low-intensity broad peak at 6.11° 2θ (*d*-spacing = 14.47 Å) and a broad shoulder at around 8.86° 2θ (*d*-spacing = 9.98 Å). In comparison with the pristine $Ti_3C_2T_x$ after annealing, where the (002) peak is again quite broad at 8.29° 2θ (*d* = 10.67 Å) with a broad shoulder at around 8.35° 2θ (10.58 Å), we can see that much of the co-intercalated water has been removed; however, this removal is not uniform, leading to these broad peaks. This same behavior was observed by Ghidiu *et al.* in studying Mg−$Ti_3C_2T_x$ at different levels of humidity.[14] In contrast, after annealing, K−$Ti_3C_2T_x$ is shifted from a 2θ of 7.08° (*d* = 12.47 Å) to 7.31° 2θ (*d* = 12.06 Å). This sharp XRD peak only shifted slightly upon annealing for K−$Ti_3C_2T_x$ as compared to that of Mg−$Ti_3C_2T_x$, which can be explained by Mg having more water per cation and less overall Mg content compared to K (because of the divalent state of the former).[14,15,41] Therefore, in the wet state, solvated Mg forms pillars causing a significant increase in *d*-spacing that collapse after annealing because the Mg content is too small to maintain the large *d*-spacing.[14,15,41] Annealed Na−$Ti_3C_2T_x$ has a broad double peak, with the first prominence at 7.20° 2θ (*d* = 12.26 Å) and the second at 8.35° 2θ (*d* = 10.58 Å), suggesting a bimodal distribution of spacing that could be due to different particle sizes within the same sample, leading to different kinetics for water removal. XRD patterns from electrodes removed from cells after 3000 cycles at 20 mV/s show that the *d*-spacings of Na- and K-intercalated $Ti_3C_2T_x$ were less affected by the vacuum annealing process. For K−$Ti_3C_2T_x$, a sharp peak at 7.16° 2θ (*d* = 12.34 Å) can be observed in addition to a small and broad peak at around 5.78° 2θ (*d* = 15.28 Å). For Na−$Ti_3C_2T_x$, much of the sample spacing recovered all the way to the pre-annealing spacing of *d* = 12.63 Å (6.99° 2θ), with a broad peak centered at 8.43° 2θ (*d* = 10.48 Å). Pristine $Ti_3C_2T_x$ recovered somewhat, with a broad peak at 7.29° 2θ (*d* = 12.11 Å) and a broad shoulder at 9.06° 2θ (*d* = 9.75 Å), while the *d*-spacing of Mg−$Ti_3C_2T_x$ increased to *d* = 12.8 Å (2θ of 6.90°) with another broad peak at 8.1° 2θ (*d* = 10.9 Å). This suggests that Na−$Ti_3C_2T_x$ and K− $Ti_3C_2T_x$ are pillared in such a way that the interlayer spacing is preserved. K−$Ti_3C_2T_x$, in particular, shows very little shifting during the annealing and rehydrating processes. Due to minor variations in sample drying, pre-annealing *d*-spacings can vary even for the same sample, but comparing the changes between pre-annealing, post-annealing, and post-cycling (*i.e.*, rehydrated) samples shows the effect of cation intercalation on maintaining the interlayer spacing.

https://doi.org/10.1021/acsaem.2c00653
ACS Appl. Energy Mater. 2022, 5, 9373−9382

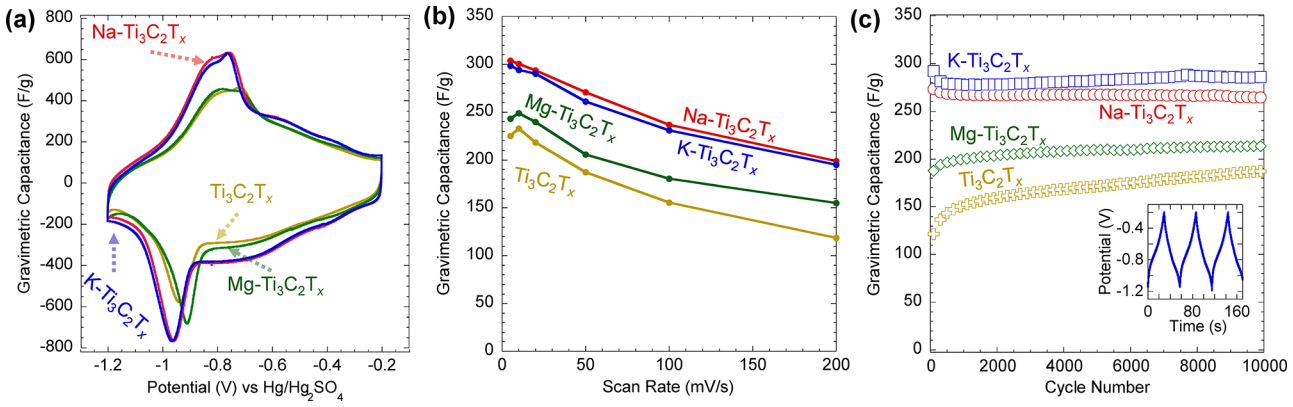

Figure 2. Electrochemical performance of pristine and pre-intercalated ~30 μm thick $Ti_3C_2T_x$ electrodes in a 1 M H_2SO_4 electrolyte. (a) Cyclic voltammogram at 5 mV/s. (b) Gravimetric capacitance at different scan rates. (c) GCPL gravimetric capacitance for 10,000 cycles at 5 A/g. The inset in (c) is a typical voltage profile *vs* Hg/Hg_2SO_4, in this case, for K−$Ti_3C_2T_x$.

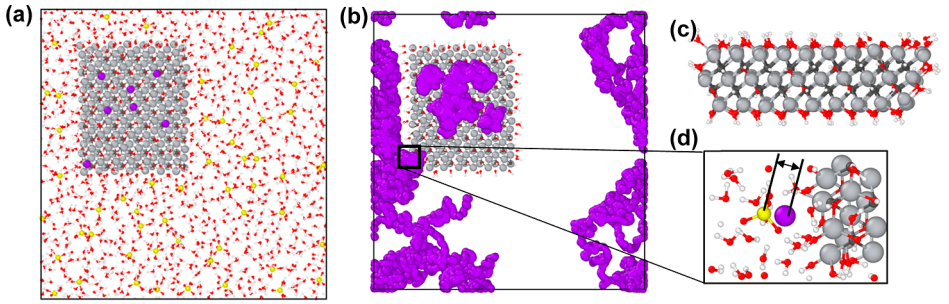

Figure 3. ReaxFF MD simulations of K^+−$Ti_3C_2T_x$ in a sulfuric acid electrolyte. (a) Full system simulated with Ti in gray, C in dark gray, O in red, H in light gray, S in yellow, and K in purple. (b) Position of all K^+ cations throughout the simulation in relation to one frame of MXene. (c) Proton-dominated termination of the MXene surface and edges. (d) Interaction between K^+ and HSO_4^- leading to the deintercalation process. The black double arrow indicates the shortest distance between the two ions at 3.97 Å.

The cyclic voltammograms at 5 mV/s shown in Figure 2a (higher scan rates are shown in Figure S1) show that Na− and K−$Ti_3C_2T_x$ have areas that are larger than those of Mg−$Ti_3C_2T_x$ and pristine $Ti_3C_2T_x$, indicating larger capacitance of both Na− and K−$Ti_3C_2T_x$ compared to the rest of the samples. Both materials (Na− and K−$Ti_3C_2T_x$) have a sharp redox peak at ~ −0.97 V during reduction and a broad peak at −0.75V during oxidation. Mg−$Ti_3C_2T_x$ and pristine $Ti_3C_2T_x$ have a less prominent broad reduction peak at ~ −0.75 V and smaller sharp peak at −0.91 V for Mg−$Ti_3C_2T_x$ and −0.95 V for $Ti_3C_2T_x$. These peaks are in similar positions to those of other $Ti_3C_2T_x$ electrodes in sulfuric acid supercapacitors and demonstrate the pseudocapacitive nature of these materials.[6,51] Previous multilayer $Ti_3C_2T_x$ MXene supercapacitors have not shown such defined redox peaks.[52] The observed peaks are shifted to a lower potential (relative to Hg/Hg_2SO_4) than redox peaks reported for $Ti_3C_2T_x$ paper electrodes (−0.8 V for reduction and −0.7 V for oxidation) and macroporous electrodes (−0.8 V for reduction and −0.75 V for oxidation).[6] These differences can be attributed to the different synthesis approaches used in these different studies similar to what was reported for MXene in Na-ion batteries.[53] Since most of the reports in the literature for MXene in H_2SO_4 electrolytes are for delaminated MXenes and the shape of the redox peaks is rarely discussed, it is not straightforward to compare the redox peaks in MXene. The difference in redox peaks' shape—in part—can be attributed to the difference between multilayer and delaminated MXenes. Another plausible reason for the shape of the redox peaks we observe here is the higher oxidation state of Ti in MXene because of pre-intercalation as discussed in our previous report.[5] It is worth noting that a similar redox peak shape was observed by Yang *et al.*[54] for nitrogen-doped urea-assisted delaminated MXene that was partially oxidized, suggesting that the shape of the peaks is related to the higher oxidation state of Ti. These comments notwithstanding, more work is needed to understand the fundamental reasons for different redox peak shapes in MXenes.

When comparing gravimetric capacitance *versus* cycling rate (Figure 2b), Na− and K−$Ti_3C_2T_x$ are comparable but much higher than the rest. On the other hand, Mg−$Ti_3C_2T_x$ and pristine $Ti_3C_2T_x$ exhibit close capacitance at low scan rates, while at a scan rate of 200 mV/s, Mg−$Ti_3C_2T_x$ exhibits an ~30% higher capacitance than pristine $Ti_3C_2T_x$. Mg−$Ti_3C_2T_x$ may show reduced rate dependance of capacitance due to its overall larger interlayer spacing when soaked in water,[14,15] facilitating the kinetics of the redox reaction. Theoretical simulations of these materials have shown that Na^+ and K^+ ions are situated very close to the outer titanium surfaces of MXene layers, whereas Mg^{2+} ions are more centrally located in the interlayer space, surrounded by a robust hydration shell.[41] These ionic locations could affect the redox processes. Indeed, XAS studies have shown that cation intercalation increases the oxidation state of titanium compared to the oxidation state of titanium in pristine $Ti_3C_2T_x$.[5] In addition, when $Ti_3C_2T_x$ is partially oxidized by heating, the capacitance is enhanced, but when it is fully oxidized, the capacitance diminishes.[51]

https://doi.org/10.1021/acsaem.2c00653
ACS Appl. Energy Mater. 2022, 5, 9373−9382

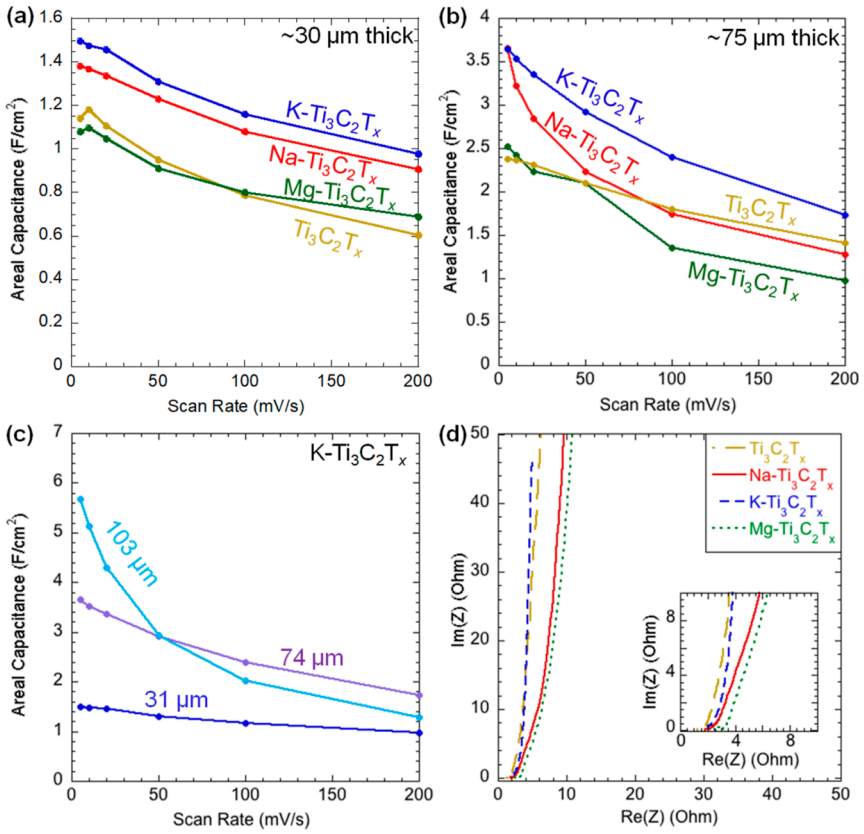

Figure 4. Areal capacitance of pristine and pre-intercalated $Ti_3C_2T_x$ electrodes with thicknesses of (a) ~ 30 μm and (b) ~ 75 μm *vs* the scan rate. (c) Areal capacitances of K−$Ti_3C_2T_x$ at thicknesses of 31, 74, and 103 μm *vs* the scan rate. (d) EIS of ~75 μm thick electrodes with the inset showing the high-frequency range.

The GCPL (Figure 2c) shows a similar trend. The voltage profiles are shown in the Figure 2c inset and Figure S2. K- and Na-intercalated $Ti_3C_2T_x$ show the highest capacitances, which are comparable to one another, with 286 F/g for K−$Ti_3C_2T_x$ and 265 F/g for Na−$Ti_3C_2T_x$. Mg−$Ti_3C_2T_x$ shows a capacitance of 214 F/g, and pristine MXene performs the worst in this test at 187.5 F/g. All four samples show very steady capacitance, with Mg−$Ti_3C_2T_x$ and pristine $Ti_3C_2T_x$ showing a slight improvement in their performance over 10,000 cycles. Favorable retention has been demonstrated in other MXene supercapacitors and further highlights the promise of MXenes in pseudocapacitive energy storage.[6,33,52] Overall, the gravimetric capacitance for K- and Na-pre-intercalated $Ti_3C_2T_x$ is much better than that of non-intercalated multilayer MXene and comparable to that of delaminated $Ti_3C_2T_x$.

Interestingly, EDS performed after 10,000 cycles of GCPL testing (Table S1) shows that most of the pre-intercalated cations are not present after the electrochemical cycling. The amount of sodium detected after cycling dropped from 0.13 Na per 3 Ti atoms to 0.05, potassium dropped from 0.11 K per 3 Ti atoms to 0.01, and Mg dropped from 0.06 Mg per 3 Ti to 0.004. Also, EDS results after 3000 cycles showed a negligible content of cations similar to what was observed after 10,000 cycles. To understand the cation removal mechanism, we used ReaxFF MD simulations to investigate K−$Ti_3C_2T_x$ as a model system for cation-intercalated MXene in a H_2SO_4 aqueous electrolyte. Figure 3a shows the system considered. Due to the protonation on the MXene surface and its edges (Figure 3b), the removal of most of the intercalated K^+ cations is likely to occur at time scales beyond that of the simulation. However, we find that the HSO_4^- ion plays a key role in mediating the removal of K^+ from the MXene interlayer. While in the absence of interactions with the HSO_4^- ions, the K^+ cation tends to retain its intercalation in the MXene interlayer (Movie SM1), the HSO_4^- ions promote the solvation of K^+ in the electrolyte and its deintercalation (Movie SM2). The ions are quickly separated after their closest approach at a K−S distance of ~3.97 Å during the deintercalation (Figure 3c), with K^+ being solvated by water molecules or different HSO_4^- ions. Figure 3d shows that the deintercalated K^+ does not reintercalate although it approaches the MXene edges at several occasions. This can be attributed to the repulsive interaction between K^+ and the MXene-edge termination, which is dominated by protons, explaining the drop in pre-intercalated cation concentration estimated by EDS after electrochemical cycling.

Despite the very low concentration of K after cycling, our XRD (Figure 1b) analyses of these materials as synthesized, after annealing, and after rehydration during electrochemical cycling show very little change to the position of the (002) peak for K−$Ti_3C_2T_x$, which was able to maintain its interlayer spacing without layer collapse, as clearly observed in the pristine and Mg−$Ti_3C_2T_x$ intercalated samples. This suggests that an extremely small amount of K is sufficient to maintain the interlayer spacing.

Where these pre-intercalated MXene electrodes fully display enhanced capacitance is in areal capacitance since much higher areal loading can be achieved for these multilayer electrodes while maintaining high gravimetric capacitance. Recently, Zheng *et al.*[55] reported an areal loading of ~10 mg/cm^2 for

https://doi.org/10.1021/acsaem.2c00653
ACS Appl. Energy Mater. 2022, 5, 9373−9382

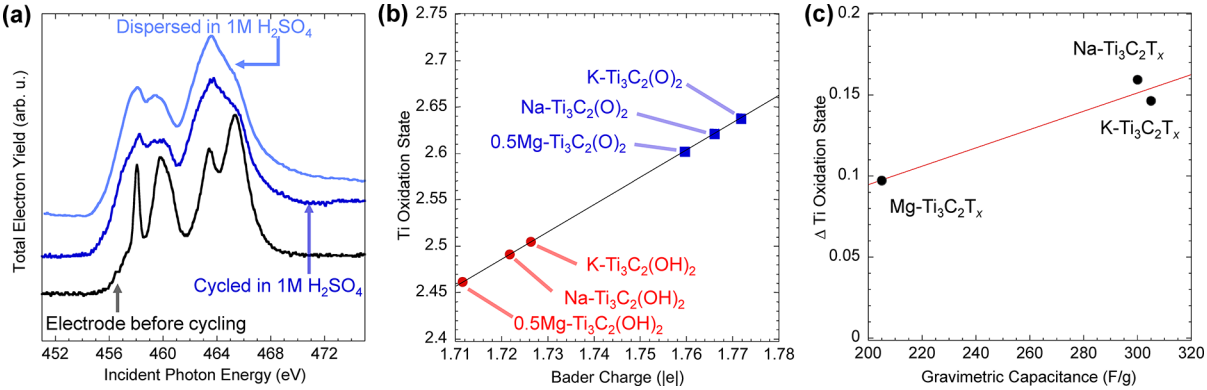

Figure 5. (a) XAS of K−$Ti_3C_2T_x$ powder dispersed in 1 M H_2SO_4, the electrode before electrochemical cycling, and the electrode removed from the cell after 3000 cycles of CV. (b) Estimated oxidation state of Ti in $Ti_3C_2T_x$ with various intercalated cations, from a linear scaling of the oxidation state *vs* Bader charge for Ti in TiO (2.0) and TiO_2 (4.0). (c) Change in the Ti oxidation state (Δ in |e|; absolute value) after protonation of the surface oxygen *vs* the measured gravimetric capacitance at 5 mV/s.

$Ti_3C_2T_x$, but the capacitance was limited to 125 F/g since the LiCl aqueous electrolyte was used, which limits the overall areal capacitance as it offers only EDLC. In our study, the 31−34 μm thick electrodes yielded capacitances of up to 1.5 F/cm^2 (Figure 4a), above previously reported values for multilayer $Ti_3C_2T_x$ (0.5 F/cm^2)[52] and $Ti_3C_2T_x$−CuCo hybrids (0.2 F/cm^2)[40] as well as for holey graphene (0.31 F/cm^2)[56] and MnO_2 (1.42 F/cm^2).[57] We then performed CV testing on thicker electrodes, which were between 70 and 77 μm thick. In these cells, areal capacitance of up to 3.7 F/cm^2 was achieved for both Na− and K−$Ti_3C_2T_x$ (Figure 4b). The gravimetric capacitances of these electrodes are shown in Figure S3. K−$Ti_3C_2T_x$ also showed the best capacitance at higher rates, maintaining a capacitance of 1.7 F/cm^2 even at 200 mV/s scan rates. The other electrode materials also showed enhanced capacitance in these thicker electrodes. Finally, we investigated a 103 μm thick K−$Ti_3C_2T_x$ with a mass loading of 20.1 mg/cm^2 and were able to reach an areal capacitance of ∼5.7 F/cm^2 (Figure 4d), which is higher than the 4.0 F/cm^2 reported for 40 μm thick $Ti_3C_2T_x$ hydrogel[6] as well as the 3.2 F/cm^2 for 48 μm thick H_2SO_4-etched $Ti_3C_2T_x$.[33]

To investigate the kinetics of different metal cation-intercalated MXenes, EIS was performed in the frequency range of 300 kHz to 10 mHz on electrodes around 75 μm thick. EIS data were simulated using the equivalent electric circuit shown in Figure S4, where R_1 and R_2 denote the system resistance and charge-transfer resistance, respectively. As shown in Figure 4c, we can observe that the system resistance increases after intercalating different metal cations. This is not surprising considering that cations are usually solvated with water, and it was reported before that inducing water and ions between the MXene sheets increases their *d*-spacing and their resistance.[14,15] In detail, Mg−$Ti_3C_2T_x$ shows the largest system resistance (2.1 Ω) and K−$Ti_3C_2T_x$ shows the smallest (1.6 Ω). This can be explained by the larger *d*-spacing of hydrated Mg−$Ti_3C_2T_x$ compared to the rest as it was shown before that the more spaced the MXene, the higher its electric resistance.[58] Pristine $Ti_3C_2T_x$, Na−$Ti_3C_2T_x$, and K−$Ti_3C_2T_x$ have a similar charge-transfer resistance (∼0.2−0.3 Ω), but Mg−$Ti_3C_2T_x$ shows a larger charge-transfer resistance (∼0.7 Ω). Compared to pristine $Ti_3C_2T_x$, Na−$Ti_3C_2T_x$, and Mg−$Ti_3C_2T_x$, K−$Ti_3C_2T_x$ exhibits the largest slope and thus the fastest diffusion. The diffusion coefficients of pristine $Ti_3C_2T_x$, Na−$Ti_3C_2T_x$, K−$Ti_3C_2T_x$, and Mg−$Ti_3C_2T_x$ are estimated to be 7.42 × 10^{-8}, 10.21 × 10^{-8}, 88.40 × 10^{-8}, and 4.93 × 10^{-8} cm^2/s, respectively. These diffusion coefficients help to explain the differences in capacitance at higher rates and increased thickness. Na−$Ti_3C_2T_x$ and K−$Ti_3C_2T_x$ behave similarly in the thinnest (∼30 μm) electrodes and at the lowest rates in the thicker (∼75 μm) electrodes, but K−$Ti_3C_2T_x$ displays a much higher performance at faster scan rates, particularly in thicker electrodes. At faster scan rates, diffusion becomes the rate-limiting step of the electrochemical reaction. Similarly, as the electrode thickness increases, faster diffusion is necessary to utilize the full electrode thickness. This increased diffusion in the K−$Ti_3C_2T_x$ electrode facilitates its ability to maintain high areal capacitance at high scan rates.

XPS was performed to understand the surface chemistry of the as-prepared powder samples with different cations (Figure S5, Table S2). The Ti 2p spectra were deconvoluted using four doublets ($2p_{3/2}$ and $2p_{1/2}$) assigned to Ti−C, Ti^{2+}, Ti^{3+}, and Ti^{4+}. The main noticeable difference between the spectra of the different samples is the intensity of the Ti^{4+} peak. The Ti^{4+} content is the highest in Mg−$Ti_3C_2T_x$ MXene, where the fraction assigned is 0.16, while this value was 0.09 for Na−$Ti_3C_2T_x$, 0.06 for K−$Ti_3C_2T_x$, and only 0.02 for $Ti_3C_2T_x$. This suggests that Mg−$Ti_3C_2T_x$ MXene has the most oxidized surface, which agrees with our previous report on XAS of intercalated $Ti_3C_2T_x$ MXene.[5] Further XPS results and discussion can be found in the Supporting Information (Figure S6 and Tables S3−S7).

To examine the effect of sulfuric acid on the oxidation state of Ti atoms in MXene, Ti L-edge XAS was performed on K−$Ti_3C_2T_x$ after dispersion in 1 M H_2SO_4 and on electrodes before and after 3000 cycles of CV at 20 mV/s (Figure 5). The XAS spectrum for the non-cycled electrode agrees well with our previously published XAS results on dried K−$Ti_3C_2T_x$ MXene prepared from an aqueous drop-cast solution.[5] The clear splitting of both L_2 (464−468 eV) and L_3 (458−462) edges is related to electronic states with t_{2g} and e_g symmetries and indicative of a high Ti oxidation state. On the other hand, the cycled MXene electrode loses the clear splitting and only a shoulder remains at both L_2 and L_3 edges. This result is interpreted as a drastic reduction of the Ti-oxidation state due to the change of the Ti−O bonding environment, probably due to hydroxylation of the MXene surface termination in an acidic environment. It has a similar signature to that of a drop-cast sample from K−$Ti_3C_2T_x$ MXene dispersed in 1 M H_2SO_4.

https://doi.org/10.1021/acsaem.2c00653
ACS Appl. Energy Mater. 2022, 5, 9373−9382

The titanium electronic structure is comparable to that of MXene exposed to a much lower H_2SO_4 concentration (0.01 M).[5] We conclude that the initially oxidized intercalated MXene electrode can be reversibly reduced upon exposure and cycling in sulfuric acid as also indicated by the shift of the L-edge onset to a lower energy. Only a small peak at around 458.1 eV remains related to a more oxidized Ti atom (Figure 5a). Even though the cations are effectively removed by electrochemical cycling (as confirmed above from EDS analysis), the highly reduced state of titanium caused by the soaking in the electrolyte post cation intercalation is maintained during cycling.

To understand how the pre-intercalated cations impact the charge storage in $Ti_3C_2T_x$ in H_2SO_4, we computed the change in the Ti oxidation state before and after protonation of the surface oxygen based on the models of $Ti_3C_2T_x$ with pre-intercalated ions. One can see from Figure 5b that Ti is more positively charged with pre-intercalated K^+, followed by Na^+ and then Mg^{2+}. More importantly, Figure 5c shows that K−$Ti_3C_2T_x$ and Na−$Ti_3C_2T_x$ have a much greater change in the Ti oxidation state than Mg−$Ti_3C_2T_x$. In other words, the computed change in the Ti oxidation suggests a greater charge storage in $Ti_3C_2T_x$ with pre-intercalated K^+ or Na^+ than with Mg^{2+}, which is in excellent agreement with the measured gravimetric capacitances (Figure 5c). While MXene surfaces can become slightly oxidized by exposure to moisture,[59] as in the aqueous salt solutions used in the intercalation procedure, our previous XAS studies show that the effects on the surface chemistries of different cation pre-intercalated $Ti_3C_2T_x$ MXenes vary with the intercalant.[5,13]

CONCLUSIONS

By the pre-intercalation of cations in multilayer MXene, we were able to achieve gravimetric capacitance of about 300 F/g in a 1 M H_2SO_4 aqueous electrolyte for multilayer Na- and K-intercalated $Ti_3C_2T_x$, which is comparable to the highest values reported for electrodes of delaminated $Ti_3C_2T_x$. This high capacitance was stable over 10,000 cycles without degradation. Exhibiting a specific capacitance for multilayer MXenes close to that of delaminated MXenes is a leap forward in MXene supercapacitor development considering that the specific surface area of multilayer MXene is typically an order of magnitude lower than that of delaminated MXene. XAS showed that oxidized Ti in pre-intercalated MXene got reduced by soaking in the H_2SO_4 electrolyte. Starting from a high oxidation state of Ti for cation-intercalated MXene, which gets reduced once protonated, can explain the high capacitance achieved here in multilayer pre-intercalated MXenes. Interestingly, this reduced state was maintained after thousands of cycles, even though de-intercalation of cations took place in the H_2SO_4 electrolyte as simulated by ReaxFF MD and proven by EDS analysis. A good agreement was found between experimentally measured capacitance, and the change of the Ti oxidation state predicted by DFT calculations for different cation pre-intercalated MXenes with Mg−$Ti_3C_2T_x$ has the lowest capacitance while Na− and K−$Ti_3C_2T_x$ have comparable capacitance.

The use of multilayer MXenes instead of delaminated MXenes allowed us to scale up the mass loading of active materials in the electrode to ∼20 mg/cm^2, achieving an electrode thickness of ∼100 μm compared to fractions of mg/cm^2 loading and few microns thick electrodes that are usually obtained for delaminated MXenes. These large values of electrode thickness and loading obtained for pre-intercalated MXene multilayers are well on par with the ∼150 μm, ∼10 mg/cm^2 thickness, and loading in commercial supercapacitor electrodes.[60] An ultra-high areal capacitance of up to 5.7 F/cm^2—the highest reported for MXenes—was achieved for multilayer K−$Ti_3C_2T_x$. These results encourage further development of multilayer MXenes by pre-intercalation to alter their properties and performance.

ASSOCIATED CONTENT

Supporting Information

The Supporting Information is available free of charge at https://pubs.acs.org/doi/10.1021/acsaem.2c00653.

EDS for intercalated $Ti_3C_2T_x$ before electrochemical cycling and after 100 cycles of galvanostatic charge/discharge testing; Ti 2p, C 1s, O 1s, and F 1s peak fitting results for $Ti_3C_2T_x$ with and without cations; Na 1s, K 2p, and Mg 2p peak fitting results for Na-$Ti_3C_2T_x$, K-$Ti_3C_2T_x$, and Mg-$Ti_3C_2T_x$, respectively; CV curves for ∼30 μm thick intercalated $Ti_3C_2T_x$; voltage profiles for Na-$Ti_3C_2T_x$, Mg-$Ti_3C_2T_x$, and pristine $Ti_3C_2T_x$; gravimetric capacitance for thicker intercalated $Ti_3C_2T_x$; equivalent electric circuit used for EIS fitting; and Ti 2p spectra and XPS spectra of $Ti_3C_2T_x$ with and without cations (PDF)

Preference of the K^+ cation to intercalate in the $Ti_3C_2T_x$ lattice in the absence of neighboring HSO_4^- in the electrolyte to enable its removal (MP4)

HSO_4^--mediated removal of K^+ from the $Ti_3C_2T_x$ lattice in a 4 M H_2SO_4 electrolyte (MP4)

AUTHOR INFORMATION

Corresponding Author

Michael Naguib − *Department of Physics and Engineering Physics, Tulane University, New Orleans, Louisiana 70118, United States;* orcid.org/0000-0002-4952-9023; Email: naguib@tulane.edu

Authors

Kaitlyn Prenger − *Department of Physics and Engineering Physics, Tulane University, New Orleans, Louisiana 70118, United States;* orcid.org/0000-0001-5654-2966

Yangunli Sun − *Department of Chemistry, University of California, Riverside, California 92521, United States*

Karthik Ganeshan − *Department of Mechanical Engineering, The Pennsylvania State University, State College, Pennsylvania 16801, United States;* orcid.org/0000-0002-3911-4246

Ameer Al-Temimy − *Helmholtz-Zentrum Berlin für Materialien und Energie GmbH, Berlin 12489, Germany; Department of Physics, Freie Universität Berlin, Berlin 14195, Germany;* orcid.org/0000-0002-4178-066X

Kun Liang − *Department of Physics and Engineering Physics, Tulane University, New Orleans, Louisiana 70118, United States*

Chaochao Dun − *The Molecular Foundry, Lawrence Berkeley National Laboratory, Berkely, California 94720, United States;* orcid.org/0000-0002-3215-6478

Jeffrey J. Urban − *The Molecular Foundry, Lawrence Berkeley National Laboratory, Berkely, California 94720, United States;* orcid.org/0000-0002-6520-830X

https://doi.org/10.1021/acsaem.2c00653
ACS Appl. Energy Mater. 2022, 5, 9373−9382

Jie Xiao − *Helmholtz-Zentrum Berlin für Materialien und Energie GmbH, Berlin 12489, Germany;* orcid.org/0000-0002-2320-6111

Tristan Petit − *Helmholtz-Zentrum Berlin für Materialien und Energie GmbH, Berlin 12489, Germany;* orcid.org/0000-0002-6504-072X

Adri C. T. van Duin − *Department of Mechanical Engineering, The Pennsylvania State University, State College, Pennsylvania 16801, United States;* orcid.org/0000-0002-3478-4945

De-en Jiang − *Department of Chemistry, University of California, Riverside, California 92521, United States;* orcid.org/0000-0001-5167-0731

Complete contact information is available at: https://pubs.acs.org/10.1021/acsaem.2c00653

Notes

The authors declare no competing financial interest.

■ ACKNOWLEDGMENTS

This research is supported by the Fluid Interface Reactions, Structures, and Transport (FIRST) Center, an Energy Frontier Research Center (EFRC) funded by the U.S. Department of Energy (DOE), Office of Science, Office of Basic Energy Sciences. This research used resources of the National Energy Research Scientific Computing Center, a DOE Office of Science User Facility supported by the Office of Science of the U.S. Department of Energy under contract no. DE-AC02-05CH11231. XPS study at the Molecular Foundry User Facility was supported by the Office of Science, Office of Basic Energy Sciences, of the U.S. Department of Energy under contract no. DE-AC01-05CH11231.

■ REFERENCES

(1) Wang, Y.; Song, Y.; Xia, Y. Electrochemical capacitors: mechanism, materials, systems, characterization and applications. *Chem. Soc. Rev.* **2016**, *45*, 5925−5950.

(2) Babu, B.; Simon, P.; Balducci, A. Fast Charging Materials for High Power Applications. *Adv. Energy Mater.* **2020**, *10*, 2001128.

(3) Simon, P.; Gogotsi, Y. Perspectives for electrochemical capacitors and related devices. *Nat. Mater.* **2020**, *19*, 1151−1163.

(4) Bélanger, D.; Brousse, T.; Long, J. W. Manganese oxides: battery materials make the leap to electrochemical capacitors. *Electrochem. Soc. Interface* **2008**, *17*, 49−52.

(5) Al-Temimy, A.; Prenger, K.; Golnak, R.; Lounasvuori, M.; Naguib, M.; Petit, T. Impact of Cation Intercalation on the Electronic Structure of Ti3C2Tx MXenes in Sulfuric Acid. *ACS Appl. Mater. Interfaces* **2020**, *12*, 15087−15094.

(6) Lukatskaya, M. R.; Kota, S.; Lin, Z.; Zhao, M.-Q.; Shpigel, N.; Levi, M. D.; Halim, J.; Taberna, P.-L.; Barsoum, M. W.; Simon, P.; Gogotsi, Y. Ultra-high-rate pseudocapacitive energy storage in two-dimensional transition metal carbides. *Nat. Energy* **2017**, *2*, 17105.

(7) Naguib, M.; Kurtoglu, M.; Presser, V.; Lu, J.; Niu, J.; Heon, M.; Hultman, L.; Gogotsi, Y.; Barsoum, M. W. Two-Dimensional Nanocrystals Produced by Exfoliation of Ti3AlC2. *Adv. Mater.* **2011**, *23*, 4248−4253.

(8) Naguib, M.; Mochalin, V. N.; Barsoum, M. W.; Gogotsi, Y. 25th anniversary article: MXenes: a new family of two-dimensional materials. *Adv. Mater.* **2014**, *26*, 992−1005.

(9) Naguib, M.; Mashtalir, O.; Carle, J.; Presser, V.; Lu, J.; Hultman, L.; Gogotsi, Y.; Barsoum, M. W. Two-dimensional transition metal carbides. *ACS Nano* **2012**, *6*, 1322−1331.

(10) Wang, H.-W.; Naguib, M.; Page, K.; Wesolowski, D. J.; Gogotsi, Y. Resolving the Structure of Ti3C2Tx MXenes through Multilevel Structural Modeling of the Atomic Pair Distribution Function. *Chem. Mater.* **2016**, *28*, 349−359.

(11) Lukatskaya, M. R.; Mashtalir, O.; Ren, C. E.; Dall'Agnese, Y.; Rozier, P.; Taberna, P. L.; Naguib, M.; Simon, P.; Barsoum, M. W.; Gogotsi, Y. Cation intercalation and high volumetric capacitance of two-dimensional titanium carbide. *Science* **2013**, *341*, 1502−1505.

(12) Deysher, G.; Shuck, C. E.; Hantanasirisakul, K.; Frey, N. C.; Foucher, A. C.; Maleski, K.; Sarycheva, A.; Shenoy, V. B.; Stach, E. A.; Anasori, B.; Gogotsi, Y. Synthesis of Mo4VAlC4 MAX Phase and Two-Dimensional Mo4VC4 MXene with Five Atomic Layers of Transition Metals. *ACS Nano* **2020**, *14*, 204−217.

(13) Al-Temimy, A.; Kronast, F.; Mawass, M.-A.; Mazzio, K. A.; Prenger, K.; Naguib, M.; Petit, T.; Raoux, S. Spatially resolved X-ray absorption spectroscopy investigation of individual cation-intercalated multi-layered Ti3C2Tx MXene particles. *Appl. Surf. Sci.* **2020**, *530*, 147157.

(14) Ghidiu, M.; Halim, J.; Kota, S.; Bish, D.; Gogotsi, Y.; Barsoum, M. W. Ion-Exchange and Cation Solvation Reactions in Ti3C2 MXene. *Chem. Mater.* **2016**, *28*, 3507−3514.

(15) Muckley, E. S.; Naguib, M.; Wang, H.-W.; Vlcek, L.; Osti, N. C.; Sacci, R. L.; Sang, X.; Unocic, R. R.; Xie, Y.; Tyagi, M.; Mamontov, E.; Page, K. L.; Kent, P. R. C.; Nanda, J.; Ivanov, I. N. Multimodality of Structural, Electrical, and Gravimetric Responses of Intercalated MXenes to Water. *ACS Nano* **2017**, *11*, 11118−11126.

(16) Osti, N. C.; Naguib, M.; Ganeshan, K.; Shin, Y. K.; Ostadhossein, A.; van Duin, A. C. T.; Cheng, Y. Q.; Daemen, L. L.; Gogotsi, Y.; Mamontov, E.; Kolesnikov, A. I. Influence of metal ions intercalation on the vibrational dynamics of water confined between MXene layers. *Phys. Rev. Mater.* **2017**, *1*, 065406.

(17) Osti, N. C.; Naguib, M.; Ostadhossein, A.; Xie, Y.; Kent, P. R. C.; Dyatkin, B.; Rother, G.; Heller, W. T.; van Duin, A. C. T.; Gogotsi, Y.; Mamontov, E. Effect of Metal Ion Intercalation on the Structure of MXene and Water Dynamics on its Internal Surfaces. *ACS Appl. Mater. Interfaces* **2016**, *8*, 8859−8863.

(18) Mashtalir, O.; Lukatskaya, M. R.; Kolesnikov, A. I.; Raymundo-Piñero, E.; Naguib, M.; Barsoum, M. W.; Gogotsi, Y. The effect of hydrazine intercalation on the structure and capacitance of 2D titanium carbide (MXene). *Nanoscale* **2016**, *8*, 9128−9133.

(19) Overbury, S. H.; Kolesnikov, A. I.; Brown, G. M.; Zhang, Z.; Nair, G. S.; Sacci, R. L.; Lotfi, R.; van Duin, A. C. T.; Naguib, M. Complexity of Intercalation in MXenes: Destabilization of Urea by Two-Dimensional Titanium Carbide. *J. Am. Chem. Soc.* **2018**, *140*, 10305−10314.

(20) Ghidiu, M.; Kota, S.; Halim, J.; Sherwood, A. W.; Nedfors, N.; Rosen, J.; Mochalin, V. N.; Barsoum, M. W. Alkylammonium Cation Intercalation into Ti3C2 (MXene): Effects on Properties and Ion-Exchange Capacity Estimation. *Chem. Mater.* **2017**, *29*, 1099−1106.

(21) Liang, K.; Matsumoto, R. A.; Zhao, W.; Osti, N. C.; Popov, I.; Thapaliya, B. P.; Fleischmann, S.; Misra, S.; Prenger, K.; Tyagi, M.; Mamontov, E.; Augustyn, V.; Unocic, R. R.; Sokolov, A. P.; Dai, S.; Cummings, P. T.; Naguib, M. Engineering the Interlayer Spacing by Pre-Intercalation for High Performance Supercapacitor MXene Electrodes in Room Temperature Ionic Liquid. *Adv. Funct. Mater.* **2021**, *31*, 2104007.

(22) Yan, L.; Zhang, B. Rose-like, ruthenium-modified cobalt nitride nanoflowers grown in situ on an MXene matrix for efficient and stable water electrolysis. *J. Mater. Chem. A* **2021**, *9*, 20758−20765.

(23) Kim, S. J.; Koh, H.-J.; Ren, C. E.; Kwon, O.; Maleski, K.; Cho, S.-Y.; Anasori, B.; Kim, C.-K.; Choi, Y.-K.; Kim, J.; Gogotsi, Y.; Jung, H.-T. Metallic Ti3C2Tx MXene Gas Sensors with Ultrahigh Signal-to-Noise Ratio. *ACS Nano* **2018**, *12*, 986−993.

(24) Muckley, E. S.; Naguib, M.; Ivanov, I. N. Multi-modal, ultrasensitive, wide-range humidity sensing with Ti3C2 film. *Nanoscale* **2018**, *10*, 21689−21695.

(25) Ying, Y.; Liu, Y.; Wang, X.; Mao, Y.; Cao, W.; Hu, P.; Peng, X. Two-dimensional titanium carbide for efficiently reductive removal of highly toxic chromium(VI) from water. *ACS Appl. Mater. Interfaces* **2015**, *7*, 1795−1803.

(26) Anasori, B.; Lukatskaya, M. R.; Gogotsi, Y. 2D metal carbides and nitrides (MXenes) for energy storage. *Nat. Rev. Mater.* **2017**, *2*, 16098.
(27) Mashtalir, O.; Naguib, M.; Mochalin, V. N.; Dall'Agnese, Y.; Heon, M.; Barsoum, M. W.; Gogotsi, Y. Intercalation and delamination of layered carbides and carbonitrides. *Nat. Commun.* **2013**, *4*, 1716.
(28) Naguib, M.; Come, J.; Dyatkin, B.; Presser, V.; Taberna, P.-L.; Simon, P.; Barsoum, M. W.; Gogotsi, Y. MXene: a promising transition metal carbide anode for lithium-ion batteries. *Electrochem. Commun.* **2012**, *16*, 61−64.
(29) Zhang, N.; Huang, S.; Yuan, Z.; Zhu, J.; Zhao, Z.; Niu, Z. Direct Self-Assembly of MXene on Zn Anodes for Dendrite-Free Aqueous Zinc-Ion Batteries. *Angew. Chem., Int. Ed.* **2021**, *60*, 2861−2865.
(30) Naguib, M.; Unocic, R. R.; Armstrong, B. L.; Nanda, J. Large-scale delamination of multi-layers transition metal carbides and carbonitrides "MXenes". *Dalton Trans.* **2015**, *44*, 9353−9358.
(31) Xie, Y.; Naguib, M.; Mochalin, V. N.; Barsoum, M. W.; Gogotsi, Y.; Yu, X.; Nam, K.-W.; Yang, X.-Q.; Kolesnikov, A. I.; Kent, P. R. C. Role of surface structure on Li-ion energy storage capacity of two-dimensional transition-metal carbides. *J. Am. Chem. Soc.* **2014**, *136*, 6385−6394.
(32) Liu, C.; Bai, Y.; Li, W.; Yang, F.; Zhang, G.; Pang, H. In Situ Growth of Three-Dimensional MXene/Metal−Organic Framework Composites for High-Performance Supercapacitors. *Angew. Chem., Int. Ed.* **2022**, *134*, No. e202116282.
(33) Tang, J.; Mathis, T.; Zhong, X.; Xiao, X.; Wang, H.; Anayee, M.; Pan, F.; Xu, B.; Gogotsi, Y. Optimizing Ion Pathway in Titanium Carbide MXene for Practical High-Rate Supercapacitor. *Adv. Energy Mater.* **2021**, *11*, 2003025.
(34) Li, S.; Chang, T.-H.; Li, Y.; Ding, M.; Yang, J.; Chen, P.-Y. Stretchable Ti3C2Tx MXene microsupercapacitors with high areal capacitance and quasi-solid-state multivalent neutral electrolyte. *J. Mater. Chem. A* **2021**, *9*, 4664−4672.
(35) Gogotsi, Y.; Simon, P. True Performance Metrics in Electrochemical Energy Storage. *Science* **2011**, *334*, 917.
(36) VahidMohammadi, A.; Mojtabavi, M.; Caffrey, N. M.; Wanunu, M.; Beidaghi, M. Assembling 2D MXenes into Highly Stable Pseudocapacitive Electrodes with High Power and Energy Densities. *Adv. Mater.* **2019**, *31*, 1806931.
(37) Zhao, S.; Liu, Z.; Xie, G.; Guo, X.; Guo, Z.; Song, F.; Li, G.; Chen, C.; Xie, X.; Zhang, N.; Sun, B.; Guo, S.; Wang, G. Achieving High-Performance 3D K + -Pre-intercalated Ti 3 C 2 T x MXene for Potassium-Ion Hybrid Capacitors via Regulating Electrolyte Solvation Structure. *Angew. Chem., Int. Ed.* **2021**, *60*, 26246−26253.
(38) Liao, L.; Wu, B.; Kovalska, E.; Mazánek, V.; Veselý, M.; Marek, I.; Spejchalová, L.; Sofer, Z. The Role of Alkali Cation Intercalates on the Electrochemical Characteristics of Nb 2 CT X MXene for Energy Storage. *Chem.—Eur. J.* **2021**, *27*, 13235−13241.
(39) Al-Temimy, A.; Anasori, B.; Mazzio, K. A.; Kronast, F.; Seredych, M.; Kurra, N.; Mawass, M.-A.; Raoux, S.; Gogotsi, Y.; Petit, T. Enhancement of Ti3C2 MXene Pseudocapacitance after Urea Intercalation Studied by Soft X-ray Absorption Spectroscopy. *J. Phys. Chem. C* **2020**, *124*, 5079−5086.
(40) Bai, Y.; Liu, C.; Chen, T.; Li, W.; Zheng, S.; Pi, Y.; Luo, Y.; Pang, H. MXene-Copper/Cobalt Hybrids via Lewis Acidic Molten Salts Etching for High Performance Symmetric Supercapacitors. *Angew. Chem., Int. Ed.* **2021**, *60*, 25318−25322.
(41) Gao, Q.; Sun, W.; Ilani-Kashkouli, P.; Tselev, A.; Kent, P. R. C.; Kabengi, N.; Naguib, M.; Alhabeb, M.; Tsai, W.-Y.; Baddorf, A. P.; Huang, J.; Jesse, S.; Gogotsi, Y.; Balke, N. Tracking ion intercalation into layered Ti3C2 MXene films across length scales. *Energy Environ. Sci.* **2020**, *13*, 2549−2558.
(42) Huang, S.; Mochalin, V. N. Hydrolysis of 2D Transition-Metal Carbides (MXenes) in Colloidal Solutions. *Inorg. Chem.* **2019**, *58*, 1958−1966.
(43) Kresse, G.; Furthmüller, J. Efficient iterative schemes forab initiototal-energy calculations using a plane-wave basis set. *Phys. Rev. B: Condens. Matter Mater. Phys.* **1996**, *54*, 11169−11186.
(44) Blöchl, P. E. Projector augmented-wave method. *Phys. Rev. B: Condens. Matter Mater. Phys.* **1994**, *50*, 17953−17979.
(45) Perdew, J. P.; Burke, K.; Ernzerhof, M. Generalized Gradient Approximation Made Simple. *Phys. Rev. Lett.* **1996**, *77*, 3865−3868.
(46) Grimme, S.; Antony, J.; Ehrlich, S.; Krieg, H. A consistent and accurate ab initio parametrization of density functional dispersion correction (DFT-D) for the 94 elements H-Pu. *J. Chem. Phys.* **2010**, *132*, 154104.
(47) Tang, W.; Sanville, E.; Henkelman, G. A grid-based Bader analysis algorithm without lattice bias. *J. Phys.: Condens. Matter* **2009**, *21*, 084204.
(48) Yu, M.; Trinkle, D. R. Accurate and efficient algorithm for Bader charge integration. *J. Chem. Phys.* **2011**, *134*, 064111.
(49) Zhan, C.; Naguib, M.; Lukatskaya, M.; Kent, P. R. C.; Gogotsi, Y.; Jiang, D.-e. Understanding the MXene Pseudocapacitance. *J. Phys. Chem. Lett.* **2018**, *9*, 1223−1228.
(50) Ganeshan, K.; Shin, Y. K.; Osti, N. C.; Sun, Y.; Prenger, K.; Naguib, M.; Tyagi, M.; Mamontov, E.; Jiang, D.-e.; van Duin, A. C. T. Structure and Dynamics of Aqueous Electrolytes Confined in 2D-TiO2/Ti3C2T2 MXene Heterostructures. *ACS Appl. Mater. Interfaces* **2020**, *12*, 58378−58389.
(51) Shao, H.; Xu, K.; Wu, Y.-C.; Iadecola, A.; Liu, L.; Ma, H.; Qu, L.; Raymundo-Piñero, E.; Zhu, J.; Lin, Z.; Taberna, P.-L.; Simon, P. Unraveling the Charge Storage Mechanism of Ti3C2Tx MXene Electrode in Acidic Electrolyte. *ACS Energy Lett.* **2020**, *5*, 2873−2880.
(52) Ghidiu, M.; Lukatskaya, M. R.; Zhao, M.-Q.; Gogotsi, Y.; Barsoum, M. W. Conductive two-dimensional titanium carbide 'clay' with high volumetric capacitance. *Nature* **2014**, *516*, 78−81.
(53) Anayee, M.; Kurra, N.; Alhabeb, M.; Seredych, M.; Hedhili, M. N.; Emwas, A.-H.; Alshareef, H. N.; Anasori, B.; Gogotsi, Y. Role of acid mixtures etching on the surface chemistry and sodium ion storage in Ti3C2Tx MXene. *Chem. Commun.* **2020**, *56*, 6090−6093.
(54) Yang, C.; Tang, Y.; Tian, Y.; Luo, Y.; Faraz Ud Din, M.; Yin, X.; Que, W. Flexible Nitrogen-Doped 2D Titanium Carbides (MXene) Films Constructed by an Ex Situ Solvothermal Method with Extraordinary Volumetric Capacitance. *Adv. Energy Mater.* **2018**, *8*, 1802087.
(55) Zheng, W.; Halim, J.; Sun, Z.; Rosen, J.; Barsoum, M. W. MXene-manganese oxides aqueous asymmetric supercapacitors with high mass loadings, high cell voltages and slow self-discharge. *Energy Storage Mater.* **2021**, *38*, 438−446.
(56) Xu, Y.; Lin, Z.; Zhong, X.; Huang, X.; Weiss, N. O.; Huang, Y.; Duan, X. Holey graphene frameworks for highly efficient capacitive energy storage. *Nat. Commun.* **2014**, *5*, 4554.
(57) He, Y.; Chen, W.; Li, X.; Zhang, Z.; Fu, J.; Zhao, C.; Xie, E. Freestanding Three-Dimensional Graphene/MnO2 Composite Networks As Ultralight and Flexible Supercapacitor Electrodes. *ACS Nano* **2013**, *7*, 174−182.
(58) Hu, T.; Zhang, H.; Wang, J.; Li, Z.; Hu, M.; Tan, J.; Hou, P.; Li, F.; Wang, X. Anisotropic electronic conduction in stacked two-dimensional titanium carbide. *Sci. Rep.* **2015**, *5*, 16329.
(59) Lotfi, R.; Naguib, M.; Yilmaz, D. E.; Nanda, J.; van Duin, A. C. T. A comparative study on the oxidation of two-dimensional Ti3C2MXene structures in different environments. *J. Mater. Chem. A* **2018**, *6*, 12733−12743.
(60) Pan, Z.; Zhi, H.; Qiu, Y.; Yang, J.; Xing, L.; Zhang, Q.; Ding, X.; Wang, X.; Xu, G.; Yuan, H.; Chen, M.; Li, W.; Yao, Y.; Motta, N.; Liu, M.; Zhang, Y. Achieving commercial-level mass loading in ternary-doped holey graphene hydrogel electrodes for ultrahigh energy density supercapacitors. *Nano Energy* **2018**, *46*, 266−276.

https://doi.org/10.1021/acsaem.2c00653
ACS Appl. Energy Mater. 2022, 5, 9373−9382